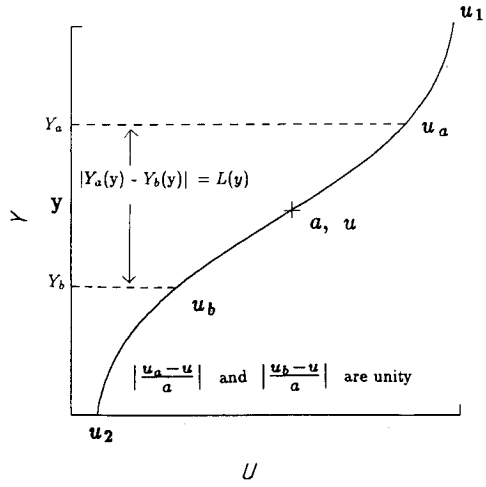

Fig. 1 Explanation of the new mixing-length concept.

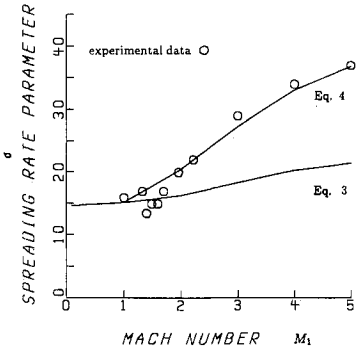

Fig. 2 Variation of spreading-rate parameter σ with Mach number.

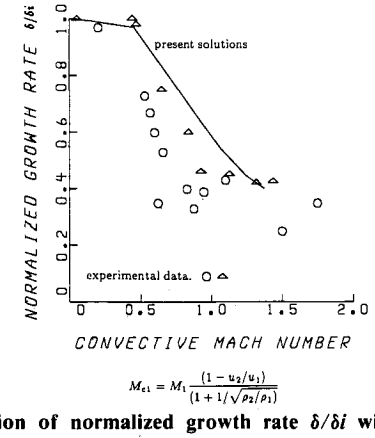

Fig. 3 Variation of normalized growth rate $\delta/\delta i$ with convective Mach number.

where X_a and X_b are axial coordinates and DY_a and DY_b are the distances between $Y_{0.9}$ and $Y_{0.1}$ at X_a and X_b, respectively. $F(=0.905)$ is a correction factor that converts the spreading rate for $u_2/u_1=0.05$ to that for $u_2/u_1=0$.

Figure 2 shows the spreading-rate parameter variations with Mach number from calculations and measurements. As seen from this figure, the new mixing-length model predicts a significant decrease of the spreading rate with increasing Mach number and the results agree well with data, while the incompressible mixing-length model gives a very small decrease of spreading rate. Figure 3 plots the variation of the normalized spreading rate with convective Mach number, and includes the experimental data compiled in Refs. 3 and 4.

The spreading-rate behavior from the new mixing-length definition shows the same trend as the experimental data. The spreading rate from the present solutions start to rapidly decrease when the convective Mach number M_{c1} is greater than 0.46 ($M_1=1$), because then a relative sonic flow exists in the shear layer.

Conclusion

A new mixing-length model was developed and applied to include the compressibility effect. The characteristic scale of the mixing region is determined locally by the lateral distance between the two points where flow moves sonic relative to the local point. Supersonic free shear layers at various Mach numbers were calculated with the new model. The results show the decrease of spreading rate with increasing Mach number and agree well with the existing experimental data.

Acknowledgment

This work was supported by the NASA Lewis Research Center under Contract NAS3-25266 with Raymond E. Gaugler as the monitor.

References

[1]Birch, S. F., and Eggers, J. M., "A Critical Review of the Experimental Data for Developed Free Turbulant Shear Layers," NASA SP-321, 1973, pp. 11-40.

[2]Brown, G. L., and Roshko, A., "On Density Effects and Large Structures in Turbulent Mixing Layers," *Journal of Fluid Mechanics*, Vol. 64, Pt. 4, 1974, pp. 775-816.

[3]Bogdanoff, D. W., "Compressibility Effects in Turbulent Shear Layers," *AIAA Journal*, Vol. 21, 1983, pp. 926, 927.

[4]Rudy, D. H., and Bushnell,D. M., "A Rational Approach to the Use of Prandtl's Mixing-Length Model in Free Turbulent Shear Flow Calculations," NASA SP-321, 1973, pp. 67-135.

[5]Crawford, M. E., and Kays, W. M., "STAN5—A Program for Numerical Computation of Two-Dimensional Internal and External Boundary-Layer Flows," NASA CR-2742, 1976.

Improvements to a Nonequilibrium Algebraic Turbulence Model

D. A. Johnson* and T. J. Coakley*
NASA Ames Research Center, Moffett Field, California 94035

Introduction

AT the Viscous Transonic Airfoil Workshop held at the AIAA 25th Aerospace Sciences Meeting at Reno, Nevada, in January 1987, Coakley[1] and King[2] both showed that the nonequilibrium turbulence model of Johnson and King[3,4] performed significantly better than the more widely used equilibrium models of Cebeci and Smith[5] and Baldwin and Lomax[6] for separated transonic airfoil flows. However, for some easier test cases where the shock wave on the upper airfoil surface was too weak to cause separation (RAE 2822 airfoil test cases 6 and 9 of Cook et al.[7]), the shock location was better predicted by the aforementioned equilibrium models.

An examination of numerical solutions for the RAE 2822 airfoil has revealed that most of the observed differences in

Received Nov. 18, 1988; revision received Aug. 16, 1989.

*Research Scientist. Associate Fellow AIAA.

predicted shock location for these weak interactions were due to a deficiency in the inner eddy viscosity formulation of the Johnson-King model. In this Note, a new formulation is presented which removes this deficiency. The new formulation satisfies the law of the wall for adverse pressure-gradient conditions better than either the original formulation or mixing-length theory. Additional modifications to the model are also presented which incorporate compressibility effects into the model and improve the prediction of skin friction for favorable and zero pressure-gradient conditions.

Turbulence Modeling

In the inner eddy viscosity formulation of the Johnson-King model, the velocity scale is proportional to the square root of the maximum Reynolds shear stress rather than to a length scale-strain rate product or a length scale vorticity product as in the Cebeci-Smith or Baldwin-Lomax models, respectively. For the weak interaction airfoil test cases considered here, this velocity scale resulted in higher wall shear levels aft of the shock wave, which in turn resulted in moderate increases ($\approx 10\%$) in boundary-layer displacement thickness near the airfoil trailing edge. Associated with these increases in boundary-layer displacement thickness were noticeably more forward shock-wave locations ($\approx 3\%$ chord).

The underlying cause for this behavior was large, near-wall eddy viscosities stemming from the use of the maximum Reynolds shear stress as the velocity scale. These large, near-wall eddy viscosities can be explained with the aid of Fig. 1. In this figure, several inner eddy viscosity distributions ν_{ti} scaled to the Johnson-King inner eddy viscosity distribution $(\nu_{ti})_{J-K}$ have been sketched as a function of y, the distance from the surface, for a hypothetical adverse pressure-gradient ($dP/dX > 0$) boundary layer. In this example, the maximum of the Reynolds shear stress τ is 2.25 times larger than the wall shear stress. The quantity u_m in this figure is the velocity scale $(-\overline{u'v'}_m)^{1/2}$ of the Johnson-King model. The subscript m denotes the location where $\tau/\rho = \overline{u'v'}$ is a maximum. For compressible flows, as will be discussed later, the velocity scale should include the density ratio $\sqrt{\rho_m/\rho}$. With this change, the inner eddy viscosity expression for the Johnson-King model is given by

$$(\nu_{ti})_{J-K} = D^2 \kappa y \sqrt{\rho_m/\rho}\, u_m \tag{1}$$

where D is a van Driest-type near-wall damping term and κ is Karman's constant.

The eddy viscosity distributions of Fig. 1 include 1) mixing-length theory as used in the Cebeci-Smith model; 2) Clauser's[8] model which uses the friction velocity u_τ as the velocity scale; and 3) a model based on the compressible law of the wall ($\partial u/\partial y = \sqrt{\rho_w/\rho}\, u_\tau/\kappa y$). The subscript w denotes wall conditions. For mixing-length theory, the substitution $\partial u/\partial y = \sqrt{\tau/\rho}/\kappa y$ has been made. Note that formulas for these distributions are given in the legend of Fig. 1. The distributions shown do not include any viscous-sublayer damping.

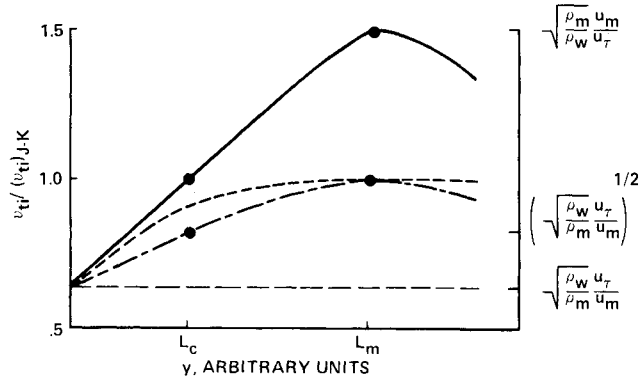

Fig. 1 Eddy viscosity distributions referenced to $(\nu_{ti})_{J-K} = \kappa y \sqrt{\rho_m/\rho}\, u_m$ (Johnson-King model) for a hypothetical adverse pressure-gradient boundary layer: —·— $\nu_{ti} = \kappa y \sqrt{\tau/\rho}$ (mixing-length theory); --- $\nu_{ti} = \kappa y \sqrt{\rho_w/\rho}\, u_\tau$ (Clauser); ——— $\nu_{ti} = \kappa y (\sqrt{\tau}/\sqrt{\rho_w} u_\tau)(\sqrt{\tau/\rho})$ (law of the wall); and ---------- ν_{ti} [Eq. (8)].

The y locations designated L_m and L_c in Fig. 1 correspond to the locations where τ/ρ is a maximum and where $\tau = \sqrt{\rho_w \rho_m}\, u_\tau u_m$, respectively. The significance of L_c is that it is where the eddy viscosities based on the law of the wall and on the Johnson-King formulas are equal. Note that for a zero pressure-gradient boundary layer, all of the eddy viscosity distributions are nearly identical for $y < L_m$ since for zero pressure-gradient conditions $\tau \approx \rho_w u_\tau^2 \approx \rho_m u_m^2$ in this region.

Near the wall ($y < L_c$), as seen from Fig. 1, the Johnson-King formula gives larger values of eddy viscosity than the other three formulas. Relative to the law of the wall, it is seen that mixing-length theory and Clauser's formula satisfy the law of the wall only very near the surface. Between L_c and the wall, the law of the wall viscosity lies between the Johnson-King viscosity and the other two viscosities.

Based on these observations and the premise that the law of the wall is more universally valid in the immediate region of the surface for attached adverse pressure-gradient conditions than is mixing-length theory[9] or the original Johnson-King formulation, a new formulation is proposed for the inner eddy viscosity distribution of the Johnson-King model. The new formulation essentially reduces to the original formulation when separation occurs. In Refs. 3 and 4, the superiority of the original formulation over mixing-length theory for separated flows was clearly demonstrated. Consistent with experiment,[9] the new formulation predicts a diminishing extent of the logarithmic region with decreasing $\tau = \sqrt{\rho_w \rho_m}\, u_\tau u_m$.

The new formulation is based on a new algebraic velocity-scale relationship whose derivation will now be presented. First, it is assumed that κy remains the proper length scale even in nonzero pressure-gradient conditions. In this case, for the law of the wall to be satisfied, the eddy viscosity velocity scale u_s must be given by

$$u_s = \frac{\sqrt{\tau}}{\sqrt{\rho_w}\, u_\tau} \sqrt{\tau/\rho} \tag{2}$$

A determinable form for the velocity scale u_s is obtained by prescribing a τ distribution for the near-wall logarithmic velocity region. The following linear distribution is believed to be reasonable:

$$\tau = \rho_w u_\tau^2 + y/L_m(\rho_m u_m^2 - \rho_w u_\tau^2) \tag{3}$$

Substituting Eq. (3) into Eq. (2) and grouping terms, the following expression is obtained for u_s:

$$u_s = \sqrt{\rho_w/\rho}\, u_\tau(1 - y/L_c') + \sqrt{\rho_m/\rho}\, u_m y/L_c' \tag{4}$$

where the term L_c' is given by

$$L_c' = \frac{\sqrt{\rho_w}\, u_\tau}{\sqrt{\rho_w}\, u_\tau + \sqrt{\rho_m}\, u_m} L_m \tag{5}$$

For the τ distribution of Eq. (3), L_c and L_c' are equivalent. To achieve the desired asymptotic value for u_s when $y/L_c' > 1$, y/L_c' in Eq. (4) is replaced by $\tanh(y/L_c')$:

$$u_s = \sqrt{\rho_w/\rho}\, u_\tau[1 - \tanh(y/L_c')] + \sqrt{\rho_m/\rho}\, u_m \tanh(y/L_c') \tag{6}$$

This completes the derivation.

The use of this velocity scale in Eq. (1) instead of $\sqrt{\rho_m/\rho}\, u_m$ is in effect a blending of the eddy viscosity relationships proposed by Clauser $(\nu_{ti})_{C1}$, and Johnson and King through the

function $\gamma_2 = \tanh(y/L_c')$:

$$\nu_{ti} = (\nu_{ti})_{C1}(1-\gamma_2) + (\nu_{ti})_{J-K}\,\gamma_2 \tag{7}$$

If $\kappa y|\,du/dy|$ is substituted for $\sqrt{\rho_w/\rho}\,u_\tau$ in Eq. (6), which is reasonable, then a blend of the mixing-length theory $(\nu_{ti})_{M-L}$ and the Johnson-King expression results:

$$\nu_{ti} = (\nu_{ti})_{M-L}(1-\gamma_2) + (\nu_{ti})_{J-K}\,\gamma_2 \tag{8}$$

In the limited experience to date, using either $\sqrt{\rho_w/\rho}\,u_\tau$ or $\kappa y\,du/dy$ in Eq. (6) yielded similar results. The use of mixing-length theory may be more easily accepted because of its extensive usage in the past. The value used for A^+ in the van Driest damping expression depends on the velocity scale. For the Clauser and Johnson-King velocity scales, a value of 17 is appropriate while for the mixing-length velocity scale a value of 26 should be used. The eddy viscosity distribution of Eq. (8) is sketched in Fig. 1.

In the intermediate calculation of L_c' from Eq. (5), u_τ is allowed to be negative, but then a lower positive limit of $0.005L_m$ is applied to L_c'. This prevents an overflow error in the computation of γ_2 when $u_\tau = 0$ and maintains a constant but very small L_c' in separated regions. To ensure a positive velocity scale in separated regions, the absolute value of u_τ is used in Eq. (6).

When the pressure gradient is favorable, the viscous sublayer extends to L_m, and mixing-length theory agrees with the law of the wall better than does the Johnson-King expression outside of L_m. Thus, for favorable pressure-gradient conditions, the argument for using Eqs. (7) or (8), based on the universality of the law of the wall, is not as strong. However, for favorable pressure-gradient cases, it has been the authors' experience that all three expressions—mixing-length theory, Clauser's expression, and the Johnson-King expression—give nearly identical results. This in part is because $\sqrt{\rho_w}\,u_\tau$ does not depart far from $\sqrt{\rho_m}\,u_m$ under favorable pressure-gradient conditions. Thus, from a pragmatic point of view, the use of Eqs. (7) and (8) in regions of favorable pressure gradient seems justified. This appears to be a better approach than setting γ_2 to zero for $dP/dX < 0$, which could result in streamwise discontinuities in ν_{ti} where dP/dX changes sign.

As noted earlier, for compressible flows $\sqrt{\rho_w/\rho}\,u_m$ should be the velocity scale in the Johnson-King inner eddy viscosity formula instead of u_m. This follows simply from the constancy of τ in a zero-pressure-gradient compressible boundary layer and the compressible law of the wall, $\partial u/\partial y = \sqrt{\rho_w/\rho}\,u_\tau/\kappa y$. This change has only a small effect for transonic flows but could be important for high supersonic flows where the ratio $\sqrt{\rho_m/\rho}$ can be far from unity. The analogy for Clauser's expression is the use of $\sqrt{\rho_w/\rho}\,u_\tau$ instead of u_τ.

Two additional modifications are suggested for the Johnson-King model to provide better predictions of skin friction for favorable and zero pressure-gradient conditions. These are 1) the use of the hyperbolic tangent function rather than an exponential in the blending of the inner ν_{ti} and outer ν_{to} eddy viscosity distributions of this model:

$$\nu_t = \nu_{to}\tanh(\nu_{ti}/\nu_{to}) \tag{9}$$

and 2) the use of u_τ or $\sqrt{\rho_m/\rho_w}\,u_m$ in the van Driest damping term, whichever is larger, rather than u_m.

Results

In Fig. 2, results for the RAE 2822 airfoil test case 9, obtained with the new inner eddy viscosity formulation of Eq. (8), are compared with the experimental data of Cook et al.[7]; the Johnson-King model results of Ref. 1; and recomputed Cebeci-Smith[5] model results. The new numerical results were obtained using the same Navier-Stokes code and grid of Ref.

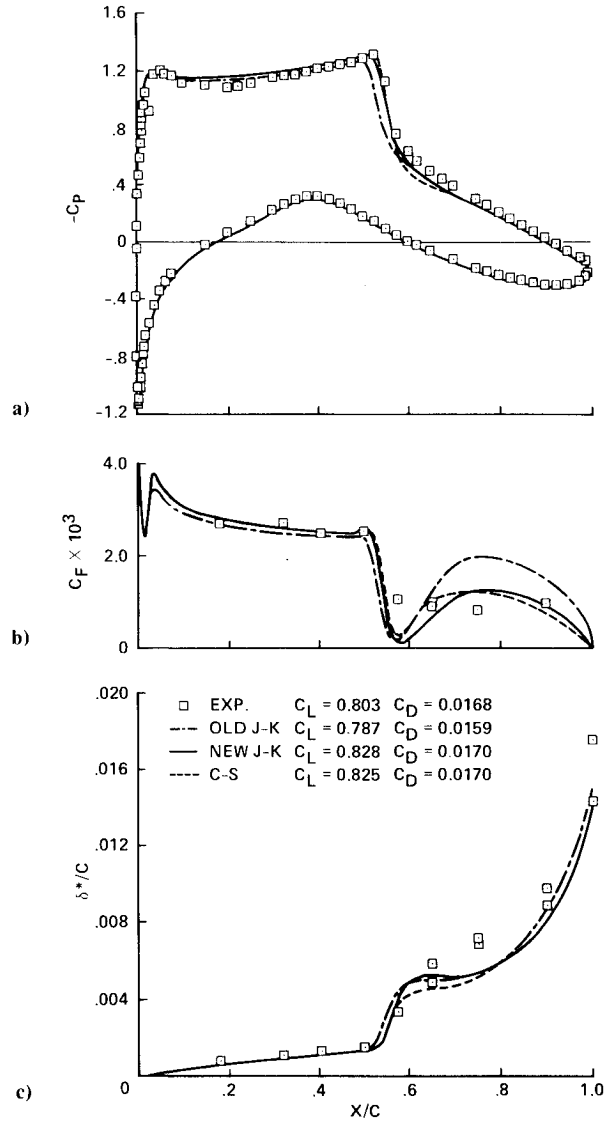

Fig. 2 RAE 2822, case 9: a) surface pressure; b) upper-surface skin friction; and c) displacement-thickness distributions at $M_{exp} = 0.729$, $M_{comp} = 0.730$, $Re = 6.5 \times 10^6$, $\alpha_{exp} = 3.19$ deg, $\alpha_{comp} = 2.8$ deg.

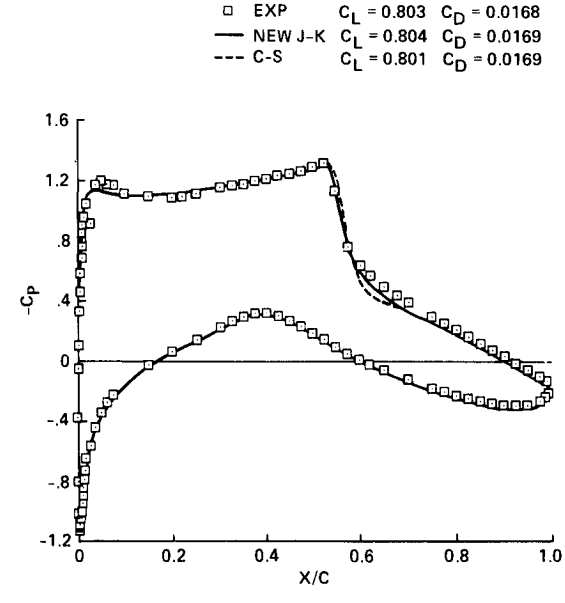

Fig. 3 RAE 2822, case 9: surface pressure distributions at $M_{exp} = 0.729$, $M_{comp} = 0.734$, $Re = 6.6 \times 10^6$, $\alpha_{exp} = 3.19$ deg, $\alpha_{comp} = 2.65$ deg.

1. In the calculations, the Mach number M was 0.73 and the angle of attack α was 2.8 deg. These are the same (corrected) conditions used by Coakley and by King. Included in Fig. 2 is a table of the lift and drag coefficients (C_L and C_D, respectively) for the calculations and the experiment. In all calculations, wall properties were used for y^+ in the van Driest damping term (i.e., $y^+ = y\rho_w u_\tau/\mu_w$). No pressure-gradient corrections for A^+ were applied.

In the *new* Johnson-King results, the diffusion term of that model was set to zero when the parameter σ of the model was less than 1. For the RAE 2822 airfoil test cases 6, 9, and 10, this change had little effect on computed results. But for the NACA 0012 airfoil, this change had a pronounced effect on predicted shock location. The original purpose of the diffusion term was to achieve better model performance in regions of flow recovery (i.e., regions where $\sigma > 1$). At the time, it was thought that the modeled diffusion term had a negligible influence in regions where σ was less than unity. Such appears not always to be the case. Considering that the validity of this term is far from established, the judicious approach is to include it only where it is known to improve the computed results—regions where σ exceeds unity.

It should be noted that the pressure rise across the shock predicted by the Johnson-King model is in better agreement with experiment than that predicted with the Cebeci-Smith model. The weaker shock is a result of a more rapid boundary-layer growth in the shock region.

For the Cebeci-Smith model solution shown in Fig. 2, the larger of the two quantities u_τ and $\sqrt{\rho_m/\rho_w}\,u_m$ was also used in the van Driest damping term. The use of simply $|u_\tau|$ instead, as has commonly been done in the implementation of the Cebeci-Smith and Baldwin-Lomax models, does not appear to be appropriate since it predicts early separation. Moreover, because of lower predicted wall shear levels on the aft section of the airfoil, it results in slower boundary-layer growth. This is accompanied by an increase in lift and a shock location that is slightly more aft in spite of the presence of separation. For the Cebeci-Smith model, C_L increases from 0.825 to 0.836 when $|u_\tau|$ alone is used in the damping term.

Because of the presence of wind-tunnel wall effects in this experiment, there is some question as to what freestream conditions should be used in the calculations. Lift and drag levels closer to those of the experiment are obtained with both the proposed modified Johnson-King model and the Cebeci-Smith modes for $M = 0.734$ and $\alpha = 2.65$ deg. A comparison of pressure distributions and a table of C_L and C_D for these conditions are presented in Fig. 3.

References

[1]Coakley, T. J., "Numerical Simulation of Viscous Transonic Airfoil Flows," AIAA Paper 87-0416, Jan. 1987.

[2]King, L. S., "A Comparison of Turbulence Closure Models for Transonic Flows About Airfoils," AIAA Paper 87-0418, Jan. 1987.

[3]Johnson, D. A., and King, L. S., "A Mathematically Simple Turbulence Closure Model for Attached and Separated Turbulent Boundary Layers," *AIAA Journal*, Vol. 23, Nov. 1985, pp. 1684-1692.

[4]Johnson, D. A., "Transonic Separated Flow Predictions with an Eddy-Viscosity/Reynolds-Stress Closure Model," *AIAA Journal*, Vol. 25, Feb. 1987, pp. 252-259.

[5]Cebeci, T., and Smith, A. M. O., *Analysis of Turbulent Boundary Layers*, Academic, New York, 1974, Chap. 6.

[6]Baldwin, B. S., and Lomax, H., "Thin-Layer Approximation and Algebraic Model for Separated Turbulent Flows," AIAA Paper 78-257, Jan. 1978.

[7]Cook, P. H., McDonald, M. A., and Firmin, M. C. P., "Aerofoil RAE 2822—Pressure Distributions, and Boundary Layer and Wake Measurements," AGARD AR-138, May 1979.

[8]Clauser, F. H., "The Turbulent Boundary Layer," *Advances in Applied Mechanics*, edited by H. L. Dryden and T. von Kármán, Vol. 4, Academic, New York, 1956, pp. 1-51.

[9]Galbraith, R. A. McD., Sjolander, S., and Head, M. R., "Mixing Length in the Wall Region of Turbulent Boundary Layers," *Aeronautical Quarterly*, Vol. 28, May 1977, pp. 97-110.

Characteristics of Hot-Film Anemometers for Use in Hypersonic Flows

Anthony Demetriades* and Scott G. Anders†
Montana State University, Bozeman, Montana 59717

TURBULENCE measurements in high-speed flows have been traditionally conducted with the hot-wire anemometer.[1] Because of the severe compressibility effects and the frequency response requirements, hot-wire signals in such flows can be interpreted only by making assumptions on the nature of the turbulence and then only by resorting to analog or digital response restoration schemes.[2] Among users of hot wires at high speeds, however, the major issue is the structural endurance of the hot wire in high-temperature, high-dynamic-pressure flows, often laden with destructive projectiles in the form of dust or liquid particles. In such an environment, the endurance problem should be eased for "hot-film" anemometers, which replace the fragile wire by a thin metallic film deposited on a rigid substrate. Some characteristics of such hot films are described in this Note.

Although hot-film anemometer probes have already been used at hypersonic speeds,[3] most of the reports on their use, and the choice one has among commercially available models, concerns applications in low-speed flows of gases and liquids[4] and low-to-moderate temperatures. Furthermore, the low-speed research gives very scant data on those basic hot-film properties that could guide the development for high-speed, high-temperature applications, long before issues of frequency response are addressed. In the present research, in addition to developing hot-film sensors capable of continuous exposure to high temperatures, measurements of the thermometric and heat-transfer properties of such typical films were made.

The present films consisted of a 0.05-cm × 0.18-cm film of platinum deposited on the stagnation line of a wedge-shaped glaze bead positioned at the tip of a 10-cm long, 0.25-cm-diam, twin-bore alumina tube.[5] Temperature endurance of each probe was checked during the fabrication process, which cycled each probe to 760°C, and in subsequent electrical stability tests in which the probe resistance was observed continuously at 730°C, typically for an hour. Probes of this design have also operated for several hours on end in the Montana State University Mach 3 wind tunnel and in the Mach 8 tunnel B of the Arnold Engineering Development Center (AEDC), where dynamic and temperature loads of 20.7 kPa and 425°C are encountered. Destructive tests pushing the film overheat to 90%, and film temperatures to 760°C have also reinforced confidence in film-probe durability.

Resistivity calibrations of these probes are routinely done in a controlled oven to determine the film resistance R dependence on the ambient temperature as represented by the "first" and "second" resistivity coefficients α and β:

$$R = R_r\left[1 + \alpha(T - T_r) + \beta(T - T_r)^2\right] \tag{1}$$

where R_r and T_r are reference conditions. In hot-wire anemometry, which historically has dealt with lower temperatures, there is little interest in or use of the β coefficient. In the present work, the calibration interval extended to 600°C to anticipate the use of the probes in hypersonic flows. As Fig. 1 shows, the resistance variation with ambient temperature is

Received Sept. 22, 1989; revision received Dec. 7, 1989; accepted for publication Dec. 19, 1989.

*Professor, Mechanical Engineering Department.

†Graduate Student, Mechanical Engineering Department.